Evidence for a Minigap in YBCO Grain Boundary Josephson Junctions

P. Lucignano,[1,2] D. Stornaiuolo,[1] F. Tafuri,[3,1] B. L. Altshuler,[4] and A. Tagliacozzo[1,5]

[1]*CNR-SPIN, Monte S. Angelo—via Cinthia, I-80126 Napoli, Italy*
[2]*International School for Advanced Studies (SISSA/ISAS), Via Beirut 2-4, I-34151 Trieste, Italy*
[3]*Dipartimento Ingegneria dell'Informazione, Seconda Università di Napoli, I-81031Aversa (CE), Italy*
[4]*Physics Department, Columbia University, 538 West 120th Street, New York, New York 10027, USA*
[5]*Dipartimento di Scienze Fisiche, Università di Napoli "Federico II," Monte S. Angelo, I-80126 Napoli, Italy*

(Received 15 June 2010; published 27 September 2010)

Self-assembled YBaCuO diffusive grain boundary submicron Josephson junctions offer a realization of a special regime of the proximity effect, where normal state coherence prevails on the superconducting coherence in the barrier region. Resistance oscillations from the current-voltage characteristic encode mesoscopic information on the junction and more specifically on the minigap induced in the barrier. Their persistence at large voltages is evidence of the long lifetime of the antinodal (high energy) quasiparticles.

DOI: 10.1103/PhysRevLett.105.147001 PACS numbers: 74.50.+r, 68.65.−k, 74.78.Na, 85.25.Am

Coherence induced by a superconductor (S) in a normal (N) region is one of the key mechanisms for transport in hybrid mesoscopic systems and characterizes the proximity effect [1–8]. The length scale hierarchy emerging from the phase coherence length L_φ, the superconducting coherence length ξ_s, the mean free path ℓ, and the size of the sample L defines the typical transport regime of the junction. When the normal state coherence dominates over the superconducting order induced in the barrier, their interplay can be encoded in the contribution of highly energetic quasiparticles (QPs) to the current with interference phenomena enhanced by size effect. Because of the d-wave order parameter symmetry [9], in high critical temperature superconductor (HTS) grain boundary Josephson junctions (GB JJs), as opposed to most traditional systems, the high values of the gap in antinodal directions set an intrinsically high energy scale for QPs, which coexist with low energy QPs. HTS are also a favorable system for the physics we address, due to their intrinsic granularity and the ease of forming "self-assembled mesocontacts or nanocontacts" across GBs. However, the results presented here are not confined to HTS only, and are general, as far as the material parameters meet the requirements $\xi_s \ll L < L_\varphi$.

We report on nonequilibrium transport measurements at low temperatures on diffusive YBaCuO GB JJs. Peculiar periodic oscillations in the resistance $R(V)$, at high voltages, are a direct manifestation of the presence of a minigap E_g in the excitation spectrum of the junctions, which arises from mesoscopic interference [6–8]. The current-voltage (I/V) characteristic keeps track of the minigap even at large voltages $V \in (7\ \mathrm{mV}, 30\ \mathrm{mV})$, due to the extremely long lifetime of the high energy carriers.

Up to now clear evidence of the minigap in low critical temperature superconducting (LTS) proximity structures has only been achieved with STM spectroscopy [3–5], but not in transport.

Our data show that QPs quantum diffuse in the constriction on a time scale $\hbar/E_c$, where $E_c = \hbar D/L^2 \sim 1$ meV is the Thouless energy, which is strongly determined by superconducting proximity at low energies.

Transport measurements have been carried out on YBaCuO off-axis biepitaxial Josephson junctions [10,11], whose structure is shown in Fig. 1 along with its model picture. Grains grow in the (103) direction on the (110) $SrTiO_3$ substrate (Fig. 1, top right), while they grow in the (001) direction on the CeO_2 seed layer (Fig. 1, bottom left). Details of the fabrication process and of complete transport characterization have been reported elsewhere [10–14]. Figure 2 condenses most of the information relevant for the arguments developed in the following. In Fig. 2(a) the I/V characteristic is reported for low voltages up to about 1.5 mV (voltage scale at the bottom). The Josephson current has a hysteresis larger than 20%, not appreciably sensitive to temperature in the range $T \in (0.3, 2)$ K. Figure 2(b) displays the switching current probability dis-

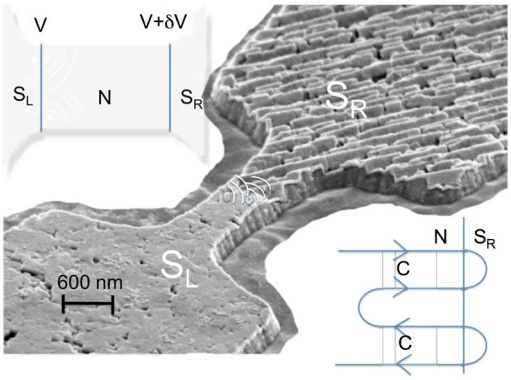

FIG. 1 (color online). Sketch of the off-axis grain boundary Josephson junction adapted from a scanning electron microscopy (SEM) picture. (103) growth (top right) has a characteristic grain shape, as compared to (001) growth (bottom left). The SEM picture refers to a typical 600 nm wide junction. Top inset: Idealized SNS junction. Bottom inset: A possible Andreev process at the N-S boundary involving the Cooperon (C) formed by the quasiparticles depicted in the barrier region.

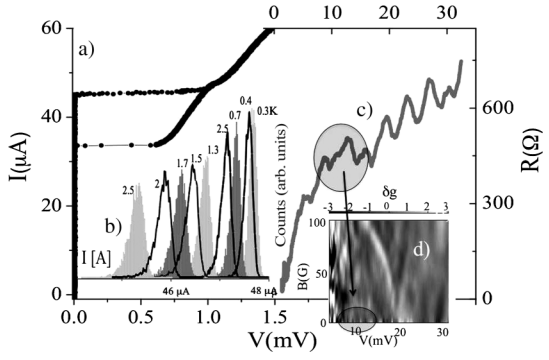

FIG. 2. (a) Current-voltage (I-V) characteristic (lower scale). (b) Switching current probability distributions versus bias current for different temperatures down to 300 mK. (c) Resistance versus voltage (voltage scale at the top). (d) Gray scale plot of the fluctuations of the dimensionless conductance as a function of the voltage V and of the applied magnetic field H at $T = 257$ mK (see [18] for details).

tributions as a function of the bias current for different temperatures down to 300 mK. The histograms follow the thermal activation behavior, confirming what it is typically observed in an hysteretic Josephson current [13,14]. The value of the voltage at which the current switches from the superconducting to the normal branch (Δ_{sw}) corresponds to the $I_C R_N$ product (I_C is the Josephson critical current and R_N is the normal state resistance), and is of the order of a few mV [15]. On the other hand, Δ_{sw} and $I_C R_N$ are an order of magnitude lower than the nominal gap value Δ, and they seem to satisfy the relation $eI_C R_N \propto E_c$ [16] rather than the usual Ambegokar-Baratoff relation $2eI_C R_N \approx \pi\Delta$.

The resistance reported in Fig. 2(c) gives neater information about the high voltage behavior (the voltage scale is at the top). The energy scale appearing in the oscillations of the resistance as a function of the voltage is also consistent with the Thouless energy E_c resulting from the magnetic response of the conductance shown in Fig. 2(d), and specifically with universal conductance fluctuations. These have been discussed in some detail in [17,18] and can be visualized in the area with more contrast in the contour plot in Fig. 2(d) around 10 meV (we have marked the corresponding voltage range in Fig. 2(c) with a gray circle). E_c matches with its expected theoretical value, which corresponds to a diffusion coefficient $D \sim 20$ cm^2/ sec and to a microbridge length of the order of $L \sim 100$ nm. E_c is quite large when compared to what is usually measured in traditional normal metal artificial systems [19,20], because our nanocontacts are self-assembled. The mesoscopic effects have been found to persist at voltages even 20 times larger than the E_c, with a reduction of the amplitude [18]. In this higher range of voltages the oscillations of the resistance fully emerge as a feature of the nonequilibrium QP transport.

We give an overview of the theoretical framework that supports our interpretation of the resistance oscillations. Because of the special "length scale hierarchy" of the device, the density of states in the constriction [Eq. (4)] displays a full minigap in the spectrum, benefiting from the specific mesoscopic single particle coherence of the sample. Mesoscopic coherence also guarantees the conditions for direct appearance of the minigap in the quasiparticle transport at relatively high voltages [Eqs. (5)–(7), and final plot in Fig. 3 along with experimental data].

At low temperatures thermal effects are negligible. The conductance only depends on elastic processes, $\propto \mathcal{T}^4$ ($\mathcal{T}$ is the tunneling matrix element). These include cotunneling, two-particle tunneling (i.e., Andreev subgap tunneling), and are contained in the Usadel equations ("dirty limit") for the diffusive QP current in the proximity regime:

$$j(r,t) = -2iD\nabla_r \int_{-\infty}^{\infty} \frac{d\omega}{2\pi} G^K(r;\omega,t). \tag{1}$$

Here $G^K(r;\omega,t)$ is the quasiclassical Keldysh Green function providing the spectral density for the supercurrent which is highly localized in energy at $E_g \ll \Delta$ [21,22]. $G^K(r;\omega,t)$ encloses the Cooperon contribution to the current, to order $1/k_F\ell$ (see inset in Fig. 1), which is the source of the enhancement of the Andreev conductance by electron interference in the diffusive N metal [23–25]:

$$\langle G^K(x_1,x_2;\omega,E)\rangle = \frac{1}{\tau}\int d^d r \langle G^K(r,r;\omega,E)\rangle \int d^d Q \times \int d^d p e^{-iQr}\langle G^R(x_1,-p;E) \times G^A(x_2,p+Q,E+\omega)\rangle \tag{2}$$

[$G^{R/A}$ are the corresponding nonequilibrium retarded or advanced single particle Green functions, and the average denotes ensemble averaging over impurity distributions and $r = (x_1 + x_2)/2$]. In stationary conditions the E dependence is dropped. $\langle G^K(r;\omega)\rangle$ satisfies the diffusion equation $D\nabla^2\langle G^K(r,\omega)\rangle = 0$ with the boundary conditions:

$$\langle G^K(r,\omega)\rangle = i\begin{cases} 2f(\omega)-1 & r=0 \\ 2f(\omega-eV)-1 & r=L, \end{cases} \tag{3}$$

where $f(\omega) = [e^{\omega/k_BT}+1]^{-1}$ is the Fermi function. In the presence of superconducting contacts, the Cooperon propagator $\Pi^C(r,Q;\omega,E) = \int d^d p \langle G^R(r,-p;E)\times G^A(r,p+Q,E+\omega)\rangle$ (Fig. 1, bottom inset) represents the proximity induced pair amplitude in the normal disordered region. In the quasiclassical approximation ($Q \sim 0$) this provides the anomalous propagator $F^R[\theta(\omega,r),\chi(\omega,r)] = \sin\theta(\omega,r)e^{i\chi(\omega,r)}$ satisfying the Usadel equations of motion [7]. The usual procedure is to solve them in the normal region ($\Delta_N = 0$) by linearization, adopting a one-dimensional space dependence and matching the solution to the superconducting order parameter at the boundary with a given phase difference $\chi_L - \chi_R$ between the two superconductors. The energy ω has an imaginary part Γ_{in} due to an inelastic scattering rate (and possibly a spin flipping rate Γ_{sf} term also).

At low temperatures, the appropriate choice for Γ_{in} in our case is the phase breaking rate [26] $\Gamma_{in} \sim 1/\tau_\varphi = D/L_\varphi^2$. Provided that this term is small and $F^R[\theta(\omega, r), \chi = 0]$ is only weakly space dependent, the density of states (DOS) in the constriction is

$$\rho(\omega) = \frac{\rho_0}{L}\int_0^L \mathrm{Re}[\cos\theta(\omega, r)]dr, \tag{4}$$

where ρ_0 is the unperturbed normal metal DOS. It displays a sharp minigap $E_g \sim 3E_c$ decreasing with increasing phase difference $\chi_L - \chi_R$ [27,28]. The analysis of the autocorrelation of the conductance fluctuations at displaced magnetic field ΔB gives an estimate of the phase coherence length $L_\varphi \lesssim 1$ μm. This is larger than the expected size of the bridge ($L_\varphi > L$), so that the condition $\Gamma_{in}/E_c = (L/L_\varphi)^2 \ll 1$ is indeed satisfied. This is quite a distinctive feature of the investigated HTS system as opposed to most of the known LTS systems.

At large voltages Andreev enhancement is lost and the contribution to conduction of the antinodal QPs can be approximated by keeping just the second order perturbation theory for sequential tunneling. The minigap, however, survives and cuts the available phase space for tunneling. We adopt a picture in which there are three regions: superconducting regions S_L and S_R and an intermediate region N with depressed superconductivity. Let us consider current from S_L to S_R. Energy labels in S_L-N-S_R are m, k, n, respectively. Defining the tunnel matrix elements $\mathcal{T}^L_{km}$:$S_L \to N$ and $\mathcal{T}^R_{kn}$:$S_R \to N$, the $S_L \to S_R$ current, to second order perturbation theory, is

$$I_{L\to R}(V) = \frac{e^2}{\hbar}\sum_{mkn}\mathcal{T}^{L*}_{kn}\mathcal{T}^R_{km}\left\{\frac{1-\tilde{f}(\epsilon_k)}{\epsilon_k - \epsilon_m} - \frac{\tilde{f}(\epsilon_k)}{\epsilon_n - \epsilon_k}\right\}(1 - f(\epsilon_n))f(\epsilon_m)\delta(\epsilon_m - \epsilon_n - \mathrm{eV}), \tag{5}$$

where $\tilde{f}(\epsilon_k)$ is the occupation probability (Fermi function) of the QP in the disordered N region ruled by the minigap E_g. At nonequilibrium and low temperatures, we approximate $\tilde{f}(\epsilon_k) \approx \exp(-|\epsilon_k - \mu_L|/E_g)$ in the first term (where μ_L is the chemical potential in the L superconductor, taken as energy reference $\epsilon_m \approx \mu_L$) and we drop the second term in the curly bracket altogether. Standard transformations [29] lead to the space representation: $I_{L\to R}(V) = \frac{e^2}{\hbar}\int dz_2 \int dy_2 \int dy_1 \int dz_1 \mathcal{T}^{R*}(y_2, z_2)\mathcal{F}(y_2, z_2, y_1, z_1) \times \mathcal{T}^L(y_1, z_1)$. where

$$\mathcal{F}(y_2, z_2, y_1, z_1) = \int_{E_g}^{eV} d\epsilon n_N(\epsilon)G^<(\epsilon - eV, z_2; \epsilon, z_1) \times \int_0^{eV-\epsilon} d\epsilon''\left\{\frac{1-\tilde{f}(\epsilon'')}{\epsilon''}\right\} \times \mathrm{Im}\{g(y_1, y_2; \epsilon'' + \epsilon)\}. \tag{6}$$

At high voltage, we can expect that the space dependent functions are only weakly energy dependent and we lump the space integrals into an average conductivity $e^2\Gamma/\hbar$, where Γ is the transmission probability through the normal region N obtained by space integration of Eq. (5). The density of states in the proximized disordered region is taken BCS-like: $n_N(\epsilon) = \mathrm{Re}\{\epsilon/\sqrt{\epsilon^2 - E_g^2}\}$. Laplace transforming the convolution of Eq. (6) to time, the full current reads

$$I(eV) = e\sqrt{\frac{E_g}{\hbar}}\mathrm{Re}\left\{\Gamma\int_{-\hbar/E_g}^{\hbar/E_g} dt\frac{\sin eVt/\hbar}{t^{3/2}}e^{-iE_gt/\hbar}\right\}. \tag{7}$$

In Fig. 3(a) the model differential resistance R is plotted as a function of V (red thin curve), with a best fit of the values of E_g and Γ to the experimental data (black bold curve). There is qualitative agreement of the oscillations in the resistance all over the resistive voltage range of the I/V characteristics. As pointed out above, the minigap E_g depends on the phase difference between $\chi_L - \chi_R$. However, in our highly nonequilibrium limit, fast oscillations of $\chi_L - \chi_R$ are expected to average the minigap to a voltage independent value. From Fig. 3(a) we find $E_g \sim$ 3.3 meV, which is consistent with a Thouless energy of $E_c \sim 1$ meV extracted from the mesoscopic features of the junction [18]. The conductance oscillations of period $\sim E_g$ over a wide voltage range $V > \Delta$ of the resistive I-V QP characteristic reveal the presence of a clear cut minigap in the nanoconstriction, and at the same time imply a very weak influence of inelastic and spin flip scattering processes. Otherwise, a sizable relaxation rate would give rise to a tail in the density of states within the minigap [which can be accounted for by an imaginary part added to E_g in Eq. (7) [4]] and determine a consequent softening of the oscillations, as shown in Fig. 3(b). This weak scattering turns into a lifetime of the QPs larger than various tens

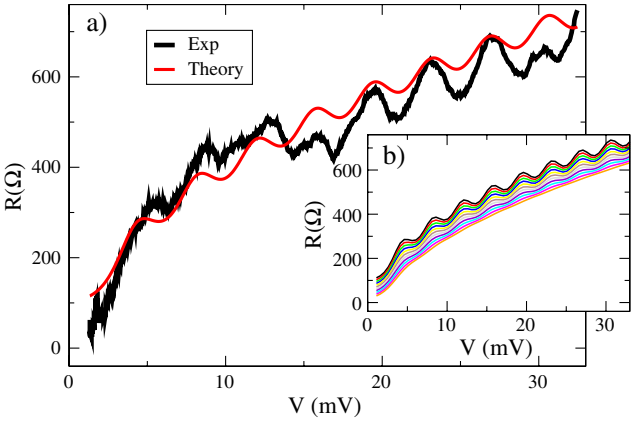

FIG. 3 (color online). (a) Measured resistance as a function of the voltage (black bold line). The red thin line is the best fit curve according to Eq. (7). The resulting minigap is $E_g \sim 3.3$ meV. (b) Decreasing the relaxation time in the Usadel equation turns the minigap into a pseudogap and softens the oscillations in the resistance. The curves are reported for increasing values of $1/\tau_\varphi \in (0, \sim\hbar/E_g)$ (from top to bottom are displaced for clarity).

of ps. This value is derived on the basis of the scattering rates we neglect to fit our data [$\hbar/E_c\tau_\varphi = (L/L_\varphi)^2$] and of the estimated $L_\varphi \sim 1$ μm, in agreement with the study on the autocorrelation function [18]. This seems to confirm the extremely long lifetime of high energy QPs in HTS, as suggested by previous experiments [13,14,30]. These values are larger than scattering times of the order of few ps measured through STM in a normal layer (Au) backed by a S (Nb), at distance up to 100 nm from the S/N interface [3,4]. Some caution is required, however, to compare systems which are structurally quite different. In Au/Nb junctions there is a real artificial interface, and STM spectra are mediated by surface effects and inhomogeneity. In GBs the S/N mismatch is intrinsic, and transport channels are substantially internal to the junctions cross section.

These conductance oscillations are expected to be quite general features of mesoscopic junctions with $\xi_s \ll L < L_\varphi$. HTS Josephson junctions allow us to access this regime which is indeed hardly achievable in LTS proximized structures. The usual proximity regime, $\xi_s > L$, in which the tail of the order parameter enters both superconductors composing the junction, does not apply to our samples. We are in the opposite limit, $\xi_s < L$, so that $\Delta > E_c$. This regime has been explored in LTS diffusive "long junctions" of conventional SNS dirty samples [2,3,5]. As opposed to our samples, in a LTS $S/N/S$ structure, the phase coherence length L_φ of Andreev reflected carriers driving the proximity is usually $L_\varphi \ll L$, so that L_φ becomes the relevant length scale in the Thouless energy: $E_c' \approx \hbar D/L_\varphi^2$. In this case the inequality required for the minigap to exist, $E_c < \Delta$, may be easily violated. In other words, we can expect that the self-averaging of the weak localization corrections in the Andreev reflection washes out the effects of the minigap in the QP's conduction. Diffusive Nb-Cu-Nb junctions with highly transparent interfaces, presumably with $L < L_\varphi$, have been measured at very low voltages $eV < E_c < \Delta$, and multiple Andreev reflections have been seen in the I/V characteristic as subgap structures [16,31]. Periodical oscillations in the magnetoconductance have recently been measured in proximized gold nanowires up to 1.2 μm long and attributed to the presence of the minigap [32]. The disappearance of those oscillations by changing the length L of the wires confirms that the showing up of the minigap is critical.

In conclusion, we have shown how the distinctive high voltage resistance oscillations, measured in YBCO GB JJs, are a fingerprint of mesoscopic effects (in particular of the minigap) and confirm long lifetime of antinodal QPs [13,14,30]. The effect is general as far as $\xi_s \ll L < L_\varphi$, which can probably also be met by specific hybrid LTS nanostructures. However, in our HTS diffusive samples, QP scattering is not only inefficient in producing relaxation in the Andreev proximity, but also in reducing the lifetime of the antinodal QPs which contribute to mesoscopic conductance fluctuations [18,30].

We acknowledge discussions with A. Barone, D. Born, F. Carillo, B. Jouault, F. Lombardi, and A. Varlamov, and financial support by MIDAS-Macroscopic Interference Devices for Atomic and Solid State Physics: Quantum Control of Supercurrents and support by European Science Foundation EUROCORES Programme FoNE, and ESF-NES.

[1] *Proceedings of the NATO Advanced Research Workshop on Mesoscopic Superconductivity, Karlsruhe, Germany, 1994*, edited by F. Hekking, G. Schön, and D. Averin [Physica (Amsterdam) 203B, 291 (1994)].
[2] S. Guéron *et al.*, Phys. Rev. Lett. **77**, 3025 (1996).
[3] M. Vinet, C. Chapelier, and F. Lefloch, Phys. Rev. B **63**, 165420 (2001).
[4] A. K. Gupta *et al.*, Phys. Rev. B **69**, 104514 (2004).
[5] H. le Sueur *et al.*, Phys. Rev. Lett. **100**, 197002 (2008).
[6] A. A. Golubov and M. Y. Kupriyanov, J. Low Temp. Phys. **70**, 83 (1988).
[7] P. Charlat *et al.*, Czech. J. Phys. **46**, 3107 (1996).
[8] W. Belzig *et al.*, Superlattices Microstruct. **25**, 1251 (1999).
[9] C. Tsuei and J. Kirtley, Rev. Mod. Phys. **72**, 969 (2000).
[10] F. Tafuri *et al.*, Phys. Rev. B **62**, 14431 (2000).
[11] F. Lombardi *et al.*, Phys. Rev. Lett. **89**, 207001 (2002).
[12] F. Tafuri and J. R. Kirtley, Rep. Prog. Phys. **68**, 2573 (2005).
[13] T. Bauch *et al.*, Science **311**, 57 (2006).
[14] T. Bauch *et al.*, Phys. Rev. Lett. **94**, 087003 (2005).
[15] D. Stornaiuolo *et al.*, J. Appl. Phys. **107**, 113901 (2010).
[16] P. Dubos *et al.*, Phys. Rev. B **63**, 064502 (2001).
[17] A. Tagliacozzo *et al.*, Phys. Rev. B **75**, 012507 (2007).
[18] A. Tagliacozzo *et al.*, Phys. Rev. B **79**, 024501 (2009).
[19] F. Pierre *et al.*, Phys. Rev. B **68**, 085413 (2003).
[20] A. van Oudenaarden *et al.*, Phys. Rev. Lett. **78**, 3539 (1997).
[21] S.-K. Yip, Phys. Rev. B **58**, 5803 (1998).
[22] T. T. Heikkilä, J. Särkkä, and F. K. Wilhelm, Phys. Rev. B **66**, 184513 (2002).
[23] A. Volkov, A. V. Zaitsev, and T. Klapwijk, Physica (Amsterdam) **210C**, 21 (1993).
[24] F. W. J. Hekking and Y. V. Nazarov, Phys. Rev. Lett. **71**, 1625 (1993).
[25] F. W. J. Hekking and Y. V. Nazarov, Phys. Rev. B **49**, 6847 (1994).
[26] I. L. Aleiner and Ya. M. Blanter, Phys. Rev. B **65**, 115317 (2002).
[27] F. Zhou *et al.*, J. Low Temp. Phys. **110**, 841 (1998).
[28] D. A. Ivanov, R. von Roten, and G. Blatter, Phys. Rev. B **66**, 052507 (2002).
[29] D. Averin and Y. Nazarov, in *Single Charge Tunneling*, edited by H. Grabert and M. Devoret, NATO Advanced Study Institutes, Ser. B Vol. 294 (Plenum, New York, 1992), p. 217.
[30] N. Gedik *et al.*, Science **300**, 1410 (2003).
[31] T. Hoss *et al.*, Phys. Rev. B **62**, 4079 (2000).
[32] J. Wang *et al.*, Phys. Rev. Lett. **102**, 247003 (2009).